参赛学生姓名： 宋秋萌

中学： 郑州一八联合国际学校

省份： 河南省

国家/地区： 中国

指导老师姓名： 葛静敏

指导老师单位： 郑州大学

论文题目： Co_3O_4/NF催化剂用于电催化糠醛氧化：性能与机理研究

参赛学生姓名： Qiumeng Song

中学： Zhengzhou No.1&8 United International School

省份： Henan

国家/地区： China

指导老师姓名： Jingmin Ge

指导老师单位： Zhengzhou University

论 文 题 目 ： Electrocatalytic Oxidation of Furfural on Co_3O_4/NF Catalyst: Performance and Mechanistic Study

Electrocatalytic Oxidation of Furfural on Co_3O_4/NF Catalyst: Performance and Mechanistic Study

Author: Qiumeng Song

Abstract

The electrocatalytic conversion of furfural (FF) into value-added chemicals like furoic acid (FA) shows significant potential for sustainable chemical production. However, understanding the catalyst's behavior during furfural oxidation remains challenging. In this study, cobalt oxide (Co_3O_4) was chosen as the model catalyst for its excellent redox properties, high activity and ease of transition between oxidation states, making it ideal for furfural electrooxidation. The Co_3O_4/NF composite demonstrated high activity and stability in furfural oxidation (FOR), achieving 80% FA selectivity and 90% Faradaic efficiency (FE) at 1.6 V vs. RHE in 30 minutes. Electrochemical tests revealed that the Co_3O_4/NF catalyst has a large electrochemical surface area (ECSA) of 58.4 mF cm^{-2}, indicating a high number of active sites. Pulse tests showed Co_3O_4 oxidizes more easily than cobalt hydroxide carbonate ($Co_2(OH)_2CO_3$) or pristine nickel foam, while broken circuit process (BCP) tests revealed that Co^{3+} species formed during electrocatalysis enhanced the spontaneous non-electrochemical oxidation rate of furfural. These results explain the catalyst's high activity and selectivity, offering insights for the design of efficient, stable electrocatalysts for biomass-derived chemicals. This study also advances understanding of surface dynamics in transition metal oxides during electrocatalysis, paving the way for next-generation catalysts.

Keywords： electrocatalysis, electrocatalytic oxidation, Co-based catalysts, furfural oxidation (FOR)

Contents

1 Introduction

The increasing demand for sustainable energy solutions has led to the exploration of renewable energy sources, such as wind, solar, hydropower and biomass, to drive critical chemical processes like water splitting for hydrogen (H_2) production. This approach offers a promising alternative to mitigate the environmental and energy challenges posed by the continued reliance on fossil fuels. However, one of the key obstacles in this process is the slow kinetics of the anodic oxygen evolution reaction (OER), which involves a complex four-electron transfer, resulting in high energy consumption. An effective strategy to reduce energy consumption is to replace OER with alternative nucleophilic oxidation reactions (NOR), such as the oxidation of hydroxyl groups and aldehydes, which can simultaneously produce value-added chemicals. Among transition-metal-based electrocatalysts, cobalt-based materials have shown significant potential for NOR. Notably, NOR has been found to be closely linked to the Co^{2+}/Co^{3+} redox reactions, yet the redox kinetics of these species and their direct impact on electrocatalytic performance remain underexplored[1-15].

In this study, we present the successful synthesis of cobalt oxide (Co_3O_4) nanoflowers directly grown on nickel foam (NF), serving as a highly efficient electrocatalyst for furfural oxidation (FOR)[16-23]. The Co_3O_4/NF composite exhibited outstanding catalytic performance, achieving an impressive 80% selectivity towards furoic acid (FA) and a high Faradaic efficiency (FE) of 90% under optimal conditions. Detailed electrochemical analysis revealed that the Co_3O_4/NF catalyst possesses a substantial electrochemical active surface area (ECSA) of 58.4 mF cm^{-2}, indicating a significant density of active catalytic sites. Furthermore, pulse testing demonstrated that Co_3O_4 undergoes oxidation more readily than cobalt hydroxide carbonate ($Co_2(OH)_2CO_3$) and pristine nickel foam, suggesting its enhanced redox properties. The optimized BCP tests further confirmed that the formation of Co^{3+} species in Co_3O_4 accelerates the spontaneous oxidation of furfural, offering a substantial improvement in reaction kinetics over $Co_2(OH)_2CO_3$ and bare NF. These findings underscore the exceptional capability of Co_3O_4/NF as a superior electrocatalyst for furfural oxidation, highlighting its potential for applications in biomass-derived chemical transformations and sustainable catalytic processes.

2 Experimental section

2.1 Materials and reagents

Hydrochloric acid (HCl, ≥37 %), ethanol, cobalt nitrate hexahydrate ($Co(NO_3)_2{\cdot}6H_2O$), urea, ammonium fluoride (NH_4F), potassium hydroxide (KOH), furfural (FF), and furoic acid (FA) were purchased from Aldrich (China). All of the reagents were used without any purification. Nickel foam (NF) was provided by HGP.

2.2 Pre-treatment of nickel foam

The pre-cleaned Nickel foam (NF) was obtained by ultrasonic cleaning for 10 minutes each with ethanol, 3 M hydrochloric acid (HCl) and deionized water to ensure the surface was free from contaminants.

2.3 Preparation of $Co_2(OH)_2CO_3$/NF

For the synthesis of $Co_2(OH)_2CO_3$/NF nanoflowers, the process began by dissolving 3 mmol cobalt nitrate hexahydrate ($Co(NO_3)_2{\cdot}6H_2O$) and 9 mmol urea in 30 mL of deionized water. This solution was stirred continuously for 30 minutes to ensure it was well-mixed and homogeneous. Next, the prepared solution was poured into a 50 mL Teflon-lined autoclave, then a piece of pre-cleaned nickel foam (NF) was fully submerged in the solution for a hydrothermal reaction. The hydrothermal process was carried out at 180°C for 12 hours.

After the hydrothermal reaction, the $Co_2(OH)_2CO_3$/NF product was thoroughly rinsed with both water and ethanol to remove any residual reactants. Finally, the cleaned material was dried under vacuum at 60°C for 6 hours to complete the synthesis. This method resulted in the successful growth of $Co_2(OH)_2CO_3$ nanoflowers on the nickel foam substrate.

2.4 Preparation of Co_3O_4/NF

For the synthesis of Co_3O_4/NF nanoflowers, the process involved a calcination process of the pre-synthesized $Co_2(OH)_2CO_3$/NF. The $Co_2(OH)_2CO_3$/NF material was placed in a muffle furnace and subjected to heat treatment at 350 °C for two hours in an air atmosphere. This controlled calcination process facilitated the oxidation of cobalt hydroxide carbonate ($Co_2(OH)_2CO_3$/NF) into cobalt oxide (Co_3O_4). The

elevated temperature in air not only ensured complete conversion but also maintained the structural integrity of the nanoflowers during the transformation. This procedure resulted in the formation of Co_3O_4 nanoflowers anchored onto the nickel foam (NF).

2.5 Characterization methods

2.5.1 Scanning electron microscopy (SEM)

SEM clearly reflects the morphological state of the catalyst. The instrument used in this paper is a JSM-7500F JEOL (5 kV) scanning electron microscope.

2.5.2 Transmission electron microscopy (TEM)

TEM is an effective characterization method for observing the morphology, particle size, and size distribution of nanoparticles. The following instruments were used: JEM-2011 TEM with an accelerating voltage of 200 kV, and an FEI Talosf 200s high-angle annular dark-field scanning transmission electron microscope (HAADF-STEM).

2.6 Electrochemical performance testing methods

2.6.1 Preparation of the working electrode

The catalyst synthesized in each experimental section was cut into a size of 1.0 cm × 1.5 cm and clamped with a platinum electrode clip, ensuring a contact area of 1.0 cm^2 with the electrolyte. This served as the working electrode, directly used for electrochemical testing.

2.6.2 Electrochemical FOR performance testing

All electrochemical tests were conducted in an H-type electrolytic cell separated by a Nafion 117 proton membrane, using a CHI660E electrochemical workstation (Shanghai Chenhua). In this study, all voltages have been converted to the potential relative to the reversible hydrogen electrode (RHE) based on the Nernst equation (Equation 2-1):

$$E\ (vs.\ RHE) = E\ (vs.\ Ag/AgCl) + 0.059 \times pH + 0.197 \quad (2\text{-}1)$$

where E (vs. RHE) represents the potential relative to the reversible hydrogen electrode, and EEE (vs. Ag/AgCl) is the electrode potential measured relative to the saturated Ag/AgCl reference electrode.

A standard three-electrode system was used to measure the electrocatalytic FOR and OER performance of the catalyst. The reference electrode was a saturated Ag/AgCl, the counter electrode was a graphite rod and the working electrode was the prepared catalyst. The electrolyte was a 1.0 M KOH solution containing 50 mM FF (or without FF). The testing conditions for linear sweep voltammetry (LSV) were a voltage range of 0-0.8 V vs. Ag/AgCl and a scan rate of 5 mV s^{-1}. The conditions for testing the electrochemical active surface area (ECSA) were a voltage range of 0.0-0.1 V vs. Ag/AgCl and scan rates of 10, 30, 50, 70, 90 and 100 mV s^{-1}. The conditions for electrochemical impedance spectroscopy (EIS) were an AC voltage amplitude of 5 mV, a frequency range of 0.01-10^5 Hz and the potential corresponding to a current density of 10 mA cm^{-2}.

3 Results

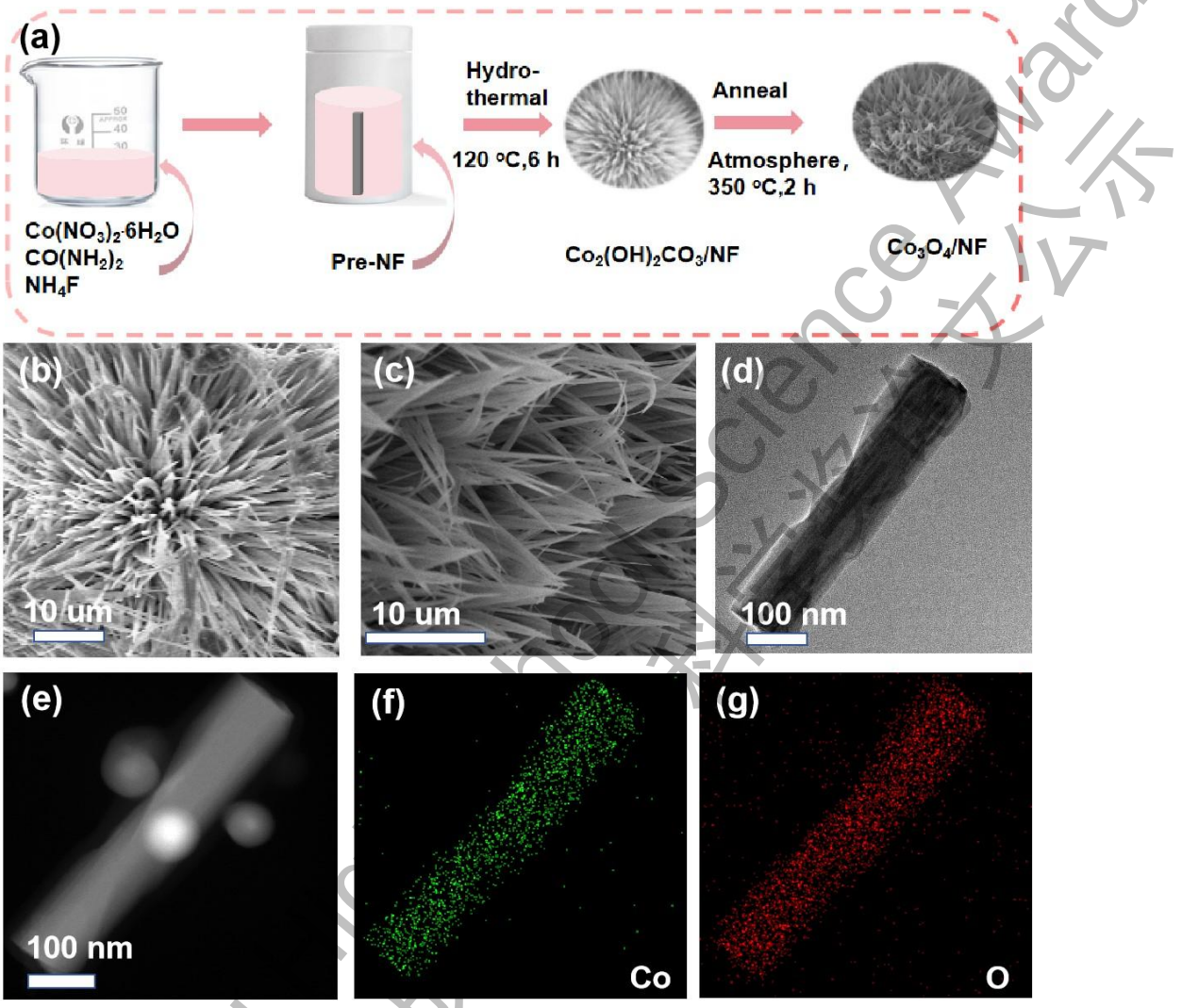

Fig.1. Synthesis and characterization of $Co_2(OH)_2CO_3$/NF and Co_3O_4/NF. (a) Schematic diagram of the synthesis process; (b) SEM image of $Co_2(OH)_2CO_3$/NF showing its nano-petal structure; (c) SEM image of Co_3O_4/NF, demonstrating the retained nano-petal morphology after oxidation; (d) TEM image of Co_3O_4/NF providing detailed structural insight; (e) STEM image of Co_3O_4/NF and corresponding elemental mappings of (f) cobalt (Co) and (g) oxygen (O).

Fig.1a illustrates the synthesis process of Co_3O_4/NF, providing an overview of the in situ growth and transformation steps. In **Fig.1b**, the SEM image of $Co_2(OH)_2CO_3$ reveals its distinctive nano-petal-like structure, characterized by thin, petal-shaped formations[24]. Similarly, **Fig.1c** shows the SEM image of Co_3O_4,

confirming that the nanostructure remains largely intact after the thermal oxidation of $Co_2(OH)_2CO_3$ in air, preserving the nano-petal morphology[25]. **Fig.1d** presents the TEM image of Co_3O_4, further corroborating the nano-petal structure at higher resolution, emphasizing its structural consistency post-calcination. The dark-field image in **Fig.1e**, along with the element mapping in **Fig.1f** and **1g**, provides critical insights into the elemental distribution. The mappings demonstrate that cobalt (Co) and oxygen (O) are uniformly distributed across the nanopetals, confirming the homogeneity of the Co_3O_4 nanoflowers[26]. This even dispersion of elements is a key factor contributing to the material's high catalytic performance, as it ensures the availability of active sites throughout the structure. These characterizations collectively highlight the stability and uniformity of the synthesized Co_3O_4/NF catalyst, which is crucial for its enhanced electrochemical activity in catalysis.

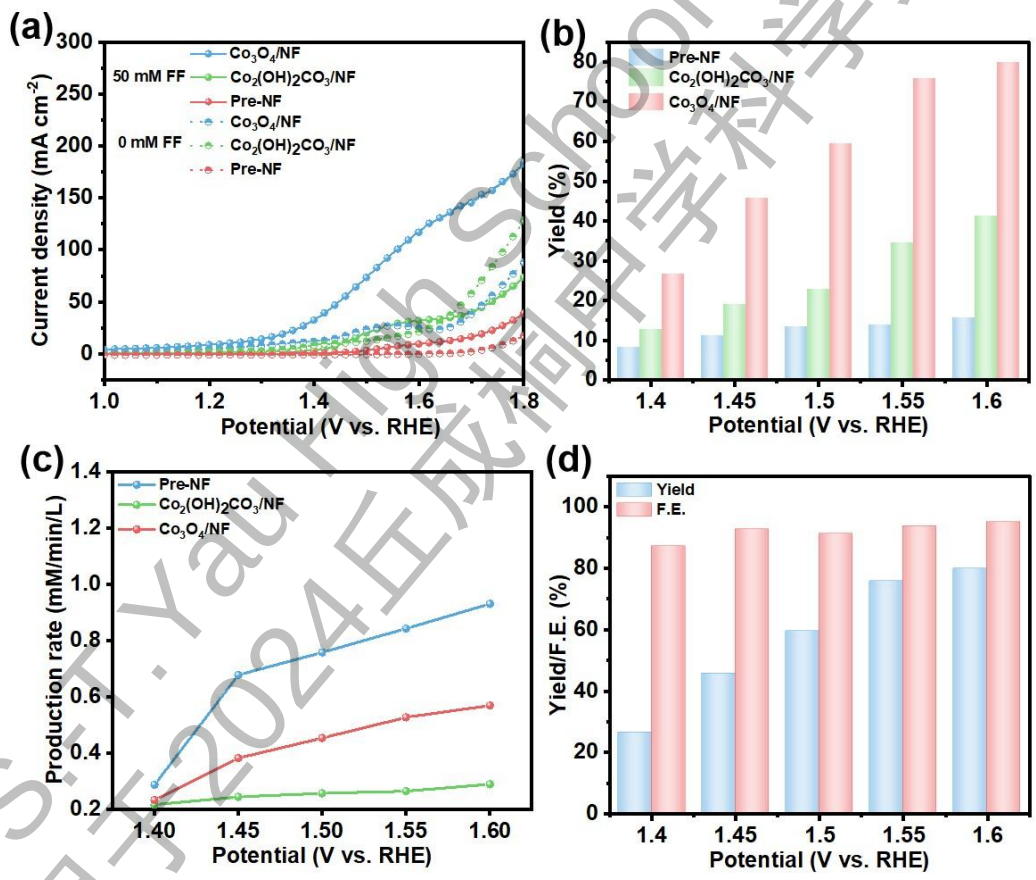

Fig.2. Furfural oxidation reaction (FOR) performance in a three-electrode system. (a) LSV curves of the three catalysts at a scan rate of 5 mV s^{-1} in 1.0 M KOH with and without 50 mM furfural (FF); (b) FA yield comparison for different catalysts; (c) FA

production rate after 30 minutes of the FOR process; (d) Faradaic efficiency (FE) and FA yield of FF oxidation over the Co_3O_4/NF catalyst after 30 minutes of FOR.

The electrocatalytic performance of the samples for furfural (FF) oxidation was evaluated using linear sweep voltammetry (LSV) under a three-electrode system. As shown in **Fig.2a**, Co_3O_4/NF demonstrated superior catalytic activity for both oxygen evolution reaction (OER) and furfural oxidation reaction (FOR) compared to $Co_2(OH)_2CO_3$/NF and pristine nickel foam (Pre-NF). Notably, the onset potential of Co_3O_4 was significantly lower than that of $Co_2(OH)_2CO_3$ and Pre-NF, indicating enhanced electrocatalytic efficiency. This lower onset potential suggests that Co_3O_4/NF requires less energy to initiate the oxidation process, contributing to its excellent catalytic performance.

Chronoamperometry tests, conducted after 30 minutes of FOR, revealed that Co_3O_4/NF exhibited a significantly higher FA yield compared to $Co_2(OH)_2CO_3$/NF and Pre-NF, as illustrated in **Fig.2b**. Interestingly, the FA yield increased with the applied potential between 1.40 V_{RHE} and 1.60 V_{RHE}, with Co_3O_4/NF reaching its maximum yield at 1.6 V_{RHE}. **Fig.2c** further highlights that the FA production rate of Co_3O_4/NF surpassed that of the other catalysts. Additionally, the system achieved over 90% Faradaic efficiency (FE) and 80% FA yield within the tested potential range, as shown in **Fig.2d**, demonstrating the excellent performance of Co_3O_4/NF in FF oxidation.

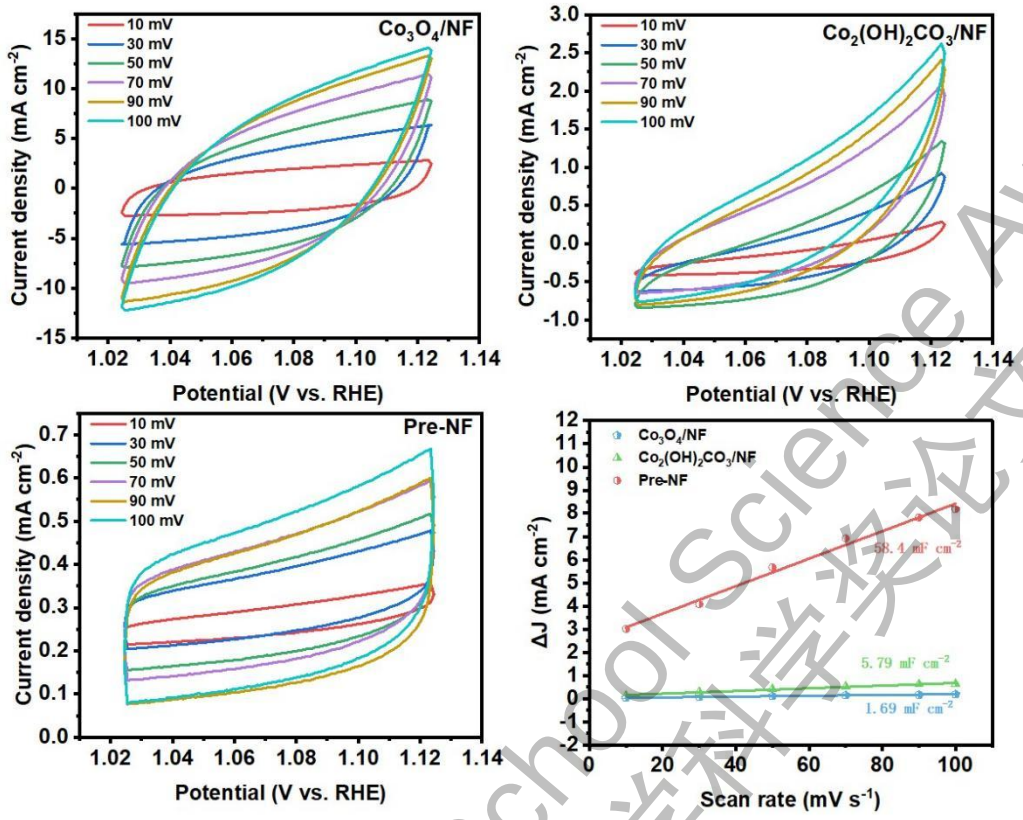

Fig.3. Cyclic voltammetry (CV) curves of furfural (FF) conversion over (a) Co_3O_4/NF, (b) $Co_2(OH)_2CO_3$/NF and (c) Pre-NF catalysts in the non-faradaic region, measured at scan rates of 10, 30, 50, 70, 90, and 100 mV s^{-1}. (d) Corresponding double-layer capacitance (Cdl) measurements at 1.07 V for all three catalysts, reflecting their electrochemical surface areas.

Fig.3 demonstrates that the electrochemical active surface area (ECSA) of Co_3O_4/NF (58.4 mF/cm²) is significantly larger than that of $Co_2(OH)_2CO_3$/NF (5.79 mF/cm²) and Pre-NF (1.69 mF/cm²). This substantial increase in active area correlates with the enhanced catalytic performance of Co_3O_4/NF, as seen in **Fig.3a**, confirming its superior activity in both furfural oxidation (FOR) and oxygen evolution reaction (OER) compared to $Co_2(OH)_2CO_3$/NF and Pre-NF. The larger ECSA suggests a greater density of active sites on Co_3O_4/NF, contributing to its heightened catalytic efficiency in these reactions.

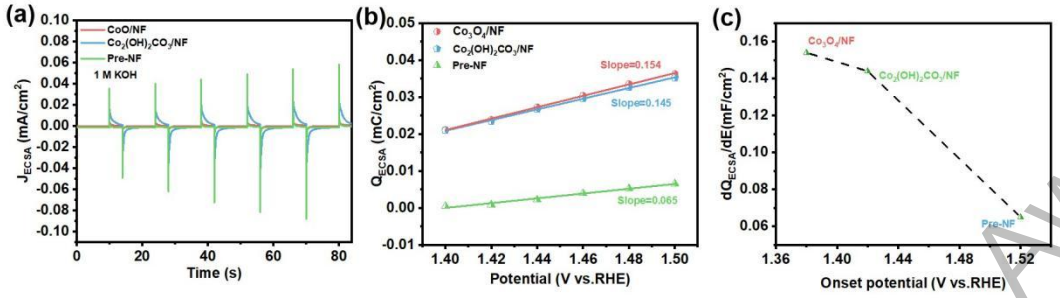

Fig.4. (a) Pulse voltammetry protocol applied between 1.15 V vs. RHE (low potential) and 1.4 V to 1.5 V vs. RHE (high potential), without iR correction. (b) Charge density (Q_{ECSA}) versus pulse voltage for different catalysts, derived from pulse-voltammetry tests. (c) The correlation between the onset potential and the deprotonation ability of the catalysts, highlighting the impact of proton removal on catalytic efficiency.

Fig.4 shows the oxidation of the catalyst during the OER process. Pulsed voltammetry tests were conducted to further assess the deprotonation ability of the catalysts. During the OER process of the Co_3O_4 catalyst in alkaline solution, $Co_2(OH)_2CO_3$ forms on the surface and subsequently deprotonates to generate Co(III)-OOH species. The deprotonation ability of the catalyst can be evaluated by measuring the charge accumulation rate on the surface under periodic pulse voltages. To ensure comparability, all electrochemical data were normalized to ECSA. As depicted in **Fig.4b**, the relationship between the total accumulated oxide charge density (Q_{ECSA}) and the pulse voltage (high potential E_h) shows a linear trend. The slope of this relationship reflects the deprotonation ability of the catalyst.

The slope values for Co_3O_4, $Co_2(OH)_2CO_3$, and Pre-NF are 0.154, 0.145, and 0.065, respectively, indicating the deprotonation capacity follows the order: Co_3O_4 > $Co_2(OH)_2CO_3$ > Pre-NF. **Fig.4c** demonstrates that the deprotonation ability of these catalysts is inversely related to their onset potential. A stronger deprotonation capacity correlates with a lower onset potential, making it easier for Co^{2+} to oxidize, thus enhancing the catalytic activity for the FOR and OER processes.

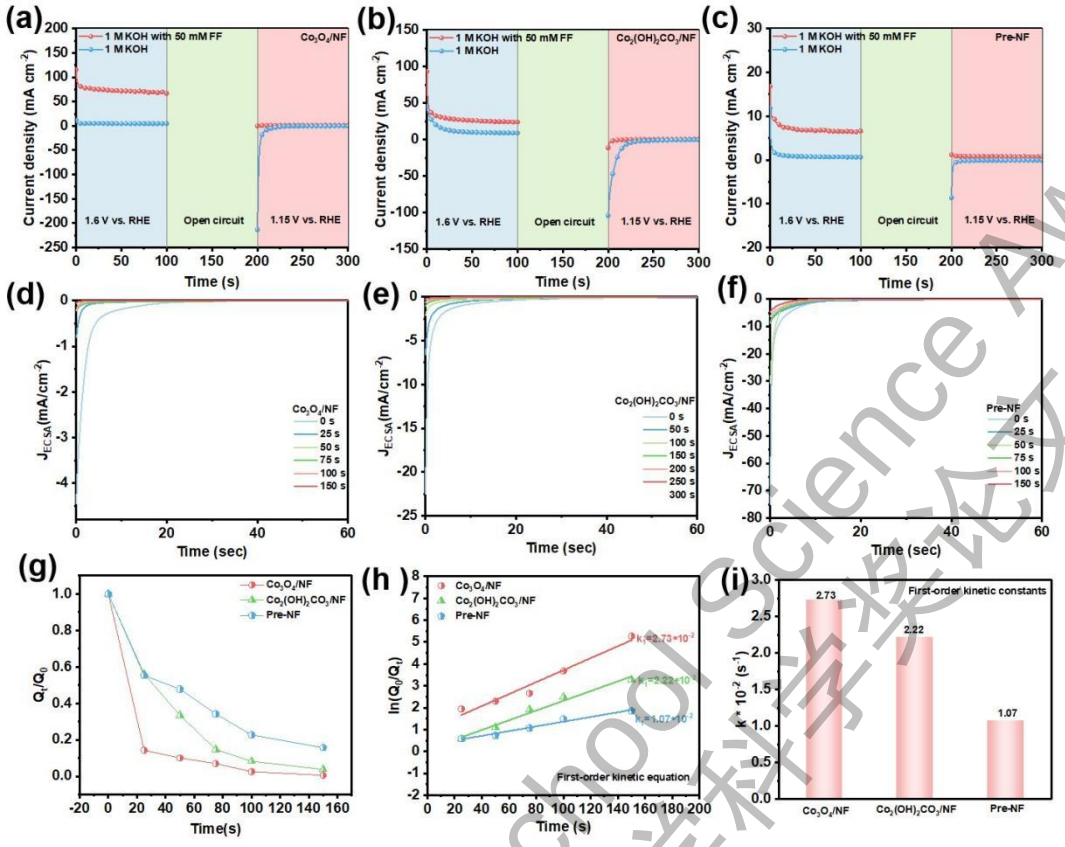

Fig.5. (a)-(c) BCP test results for Co_3O_4 ,$Co_2(OH)_2CO_3$ and Pre-NF, respectively; (d)-(f) Multi-potential step measurements for Co_3O_4, $Co_2(OH)_2CO_3$ and Pre-NF in 1.0 M KOH solution, both with and without the presence of 50 mM FF. 5(g) Schematic diagram of the BCP tests in KOH-FF solution, which were designed to evaluate the reaction kinetics of furfural (FF) with the active intermediate species (Co(III)-OOH). (h) the plots of Q_t/Q_0 versus time (t), derived from the optimized BCP-KOH-FF tests, 5(i) the corresponding linear fitting of kinetic constants using a first-order kinetics equation for Co_3O_4, $Co_2(OH)_2CO_3$ and Pre-NF catalysts.

To investigate the effect of spontaneous non-electrochemical reactions on FOR activity, BCP tests were employed to analyze differences in spontaneous chemical reaction kinetics. **Fig.5a-c** present the BCP test results for Co_3O_4, $Co_2(OH)_2CO_3$ and Pre-NF, respectively. During the BCP process in 1 M potassium hydroxide (KOH) solution (BCP-KOH), all catalysts showed a discharge curve at low potential due to surface charge accumulation at high potential, forming Co(III)-OOH. The discharge magnitude followed the order: Co_3O_4 > $Co_2(OH)_2CO_3$ > Pre-NF, indicating greater surface charge accumulation of Co(III)-OOH in Co_3O_4. However, when the BCP

process was conducted in 1 M KOH with 50 mM FF (BCP-FF), the discharge curve disappeared, suggesting a spontaneous non-electrochemical reaction between Co(III)-OOH and FF during the FOR process.

To quantitatively assess the kinetics of these spontaneous reactions, an optimized BCP-KOH-FF process was designed (**Fig.5g**). The test involved double-segment amperometric i-t measurements. First, under a high potential of 1.60 V vs. RHE in 1 M KOH solution, the charging process lasted 100 s. This was followed by a BCP process in 1 M KOH + 50 mM FF solution and a final discharge at a low potential of 1.15 V vs. RHE for 60 s. The discharge i-t curve reflected the reduction of Co(III)-OOH, and the discharge quantity (Q_t) was calculated by integrating the discharge current.

By varying the BCP duration, Q_t-t curves were obtained, revealing the spontaneous reaction rates: Co_3O_4 > $Co_2(OH)_2CO_3$> Pre-NF (**Fig.5h**). Using the first-order kinetic equation $\ln(Q_0/Q_t) = kt$, where k is the rate constant, the linear fitting results confirmed the order of reaction kinetics: Co_3O_4 > $Co_2(OH)_2CO_3$ > Pre-NF (**Fig.5i**).

The pulse test in **Fig.4** and the BCP test in **Fig.5** indicate that, compared to $Co_2(OH)_2CO_3$ and Pre-NF, Co_3O_4 exhibits easier electrooxidation and faster kinetics in the spontaneous oxidation of FF.

4 Conclusion

In conclusion, we have successfully employed Co_3O_4/NF as a model catalyst to investigate its exceptional catalytic performance in furfural oxidation, providing valuable insights into the underlying mechanisms driving its high activity. Our comprehensive electrochemical analysis revealed that Co_3O_4 exhibits remarkable selectivity (~80%) for furoic acid (FA) production and a Faradaic efficiency (FE) of approximately 90% under alkaline conditions, demonstrating its potential for sustainable chemical synthesis. The cobalt oxide nanoflowers displayed an impressive electrochemical active surface area (ECSA) of 58 mF cm^{-2}, confirming the high density of catalytic sites available for reaction.

Moreover, pulse tests showed that Co_3O_4 undergoes oxidation more readily than its counterparts, $Co_2(OH)_2CO_3$ and pristine nickel foam (Pre-NF), further enhancing its electrocatalytic activity. The results from both the standard and optimized BCP tests provided critical evidence that Co_3O_4 facilitates the spontaneous oxidation of

furfural at a significantly faster rate than $Co_2(OH)_2CO_3$ and Pre-NF, emphasizing the superior kinetics of Co_3O_4 in the reaction process.

These findings not only highlight Co_3O_4's superior catalytic performance but also offer a clearer understanding of how its intrinsic properties, such as redox flexibility and deprotonation ability, contribute to enhanced reactivity. This study paves the way for the development of advanced electrocatalysts for biomass-derived chemical transformations and holds promise for future innovations in energy-efficient catalytic processes.

5 Potential further experiments

Further mechanistic studies could be carried out using in situ spectroscopic techniques. These techniques includes Raman spectroscopy, X-ray absorption near-edge structure (XANES) and infrared (IR) spectroscopy. They could be employed during the electrocatalytic reactions to monitor the oxidation states of Co_3O_4. This would provide deeper insights into the reaction mechanism, particularly the formation and role of intermediate species such as Co(III)-OOH during the oxidation process.

Moreover, creating intentional distortions in the crystal structure of Co_3O_4 to influence d-orbital splitting and improve its catalytic performance also is an intriguing experimental direction. Distortion in the crystal lattice can lead to the formation of $d_{x^2-y^2}$ orbital with a higher energy level. This means the $d_{x^2-y^2}$ orbital will be closer to the Fermi level and hence the catalyst will have a stronger deprotonation ability. We can achieve this by either cation doping or creating oxygen vacancies in the Co_3O_4 lattice. The impact can be characterized using techniques like X-ray diffraction (XRD) and X-ray photoelectron spectroscopy (XPS) etc.

References

[1] Alothman, A. A.; Jabbour, K.; Manzoor, S.; Abid, A. G.; Nisa, M. U.; Gomez, P. H.; Wabaidur, S. M.; Sillanpää, M. Facile fabrication of CuScS2/CoO as an efficient electrocatalyst for oxygen evolution reaction and water treatment process. International Journal of Hydrogen Energy 2024, 49, 564-579. DOI: 10.1016/j.ijhydene.2023.08.215.

[2] Dang, Y.; Li, X.; Chen, Z.; Ma, B.; Zhao, X.; Chen, Y. Hierarchical CoO@MoN heterostructure nanowire array as a highly efficient electrocatalyst for hydrogen evolution. Chemical Engineering Journal 2023, 477. DOI: 10.1016/j.cej.2023.147154.

[3] Diao, L.; Zhou, W.; Zhang, B.; Shi, C.; Miao, Z.; Zhou, J.; He, C. NaCl sealing Strategy-Assisted synthesis CoO-Co heterojunctions as efficient oxygen electrocatalysts for Zn air batteries. Journal of Colloid and Interface Science 2023, 645, 329-337. DOI: 10.1016/j.jcis.2023.04.080.

[4] Du, T.; Gao, Y.; Liu, Z.; Chen, T.; Zhang, X.; Yang, F. CoO/NiFe LDH heterojunction as a photo-assisted electrocatalyst for efficient oxygen evolution reaction. International Journal of Hydrogen Energy 2024, 51, 907-915. DOI: 10.1016/j.ijhydene.2023.09.040.

[5] Guo, J.-X.; Yan, D.-Y.; Qiu, K.-W.; Mu, C.; Jiao, D.; Mao, J.; Wang, H.; Ling, T. High electrocatalytic hydrogen evolution activity on a coupled Ru and CoO hybrid electrocatalyst. Journal of Energy Chemistry 2019, 37, 143-147. DOI: 10.1016/j.jechem.2018.12.011.

[6] Ran, J.; Si, M.; Gao, D. Co@CoO chiral nanostructures enabling efficient oxygen electrocatalysis by modulated spin-polarization. Chemical Engineering Journal 2024, 493. DOI: 10.1016/j.cej.2024.152545.

[7] Ren, X.; Hou, F.; Wang, F.; Zhang, X.; Wang, Q. Porous CoO-CeO2 heterostructures as highly active and stable electrocatalysts for water oxidation. International Journal of Hydrogen Energy 2018, 43 (50), 22529-22537. DOI: 10.1016/j.ijhydene.2018.10.096.

[8] Wang, C.; Li, Y.; Gu, C.; Zhang, L.; Wang, X.; Tu, J. Active Co@CoO core/shell nanowire arrays as efficient electrocatalysts for hydrogen evolution reaction. Chemical Engineering Journal 2022, 429. DOI: 10.1016/j.cej.2021.132226.

[9] Zhang, H.; Li, W.; Feng, X.; Chen, N.; Zhang, H.; Zhao, X.; Wang, L.; Li, Z. Interfacial FeOOH/CoO nanowires array improves electrocatalytic water splitting. Journal of Solid State Chemistry 2021, 298. DOI: 10.1016/j.jssc.2021.122156.

[10] Zhang, K.; Xia, X.; Deng, S.; Xie, D.; Lu, Y.; Wang, Y.; Wu, J.; Wang, X.; Tu, J. N-doped CoO nanowire arrays as efficient electrocatalysts for oxygen evolution reaction. Journal of Energy Chemistry 2019, 37, 13-17. DOI: 10.1016/j.jechem.2018.11.013.

[11] Chen, S.; Qi, G.; Yin, R.; Liu, Q.; Feng, L.; Feng, X.; Hu, G.; Luo, J.; Liu, X.; Liu, W. Electrocatalytic nitrate-to-ammonia conversion on CoO/CuO nanoarrays using Zn–nitrate batteries. *Nanoscale* **2023**, *15* (48), 19577-19585. DOI: 10.1039/d3nr05254k.

[12] Chu, K.; Liu, Y.-p.; Li, Y.-b.; Zhang, H.; Tian, Y. Efficient electrocatalytic N2 reduction on CoO quantum dots. *Journal of Materials Chemistry A* **2019**, *7* (9), 4389-4394. DOI: 10.1039/c9ta00016j.

[13] Gan, J.; Huang, Z.; Luo, W.; Chen, W.; Cao, Y.; Qian, G.; Zhou, X.; Duan, X. Platelet carbon nanofibers as support of Pt-CoO electrocatalyst for superior hydrogen evolution. *Journal of Energy Chemistry* **2021**, *52*, 33-40. DOI: 10.1016/j.jechem.2020.04.036.

[14] Hu, Z.; Zhou, Y.; Wu, C.; Cheng, L.; Tai, Y.; Chen, S.; Song, L.; Ge, B. Exploring the Formation of CoO/ZnO Heterostructure to Enhance Electrocatalytic Oxygen Evolution Reaction. *Advanced Materials Interfaces* **2023**, *10* (16). DOI: 10.1002/admi.202300091.

[15] Huang, X.; Song, J.; Hua, M.; Xie, Z.; Liu, S.; Wu, T.; Yang, G.; Han, B. Enhancing the electrocatalytic activity of CoO for the oxidation of 5-hydroxymethylfurfural by introducing oxygen vacancies. *Green Chemistry* **2020**, *22* (3), 843-849. DOI: 10.1039/c9gc03698a.

[16] Liang, Z.; Huang, Z.; Yuan, H.; Yang, Z.; Zhang, C.; Xu, Y.; Zhang, W.; Zheng, H.; Cao, R. Quasi-single-crystalline CoO hexagrams with abundant defects for highly efficient electrocatalytic water oxidation. *Chemical Science* **2018**, *9* (34), 6961-6968. DOI: 10.1039/c8sc02294a.

[17] Liu, X.; Dong, C.; Dong, W.; Wang, X.; Yuan, X.; Huang, F. Co nanoparticles embedded in a 3D CoO matrix for electrocatalytic hydrogen evolution. *RSC Advances* **2016**, *6* (45), 38515-38520. DOI: 10.1039/c6ra07538j.

[18] Qi, J.; Zhang, W.; Cao, R. Aligned cobalt-based Co@CoOx nanostructures for efficient electrocatalytic water oxidation. *Chemical Communications* **2017**, *53* (66), 9277-9280. DOI: 10.1039/c7cc04609j.

[19] Wang, N.; Chen, B.; Qin, K.; Liu, E.; Shi, C.; He, C.; Zhao, N. Rational design

of Co9S8/CoO heterostructures with well-defined interfaces for lithium sulfur batteries: A study of synergistic adsorption-electrocatalysis function. *Nano Energy* **2019**, *60*, 332-339. DOI: 10.1016/j.nanoen.2019.03.060.

[20] Zhou, Q.; Sun, R.; Ren, Y.; Tian, R.; Yang, J.; Pang, H.; Huang, K.; Tian, X.; Xu, L.; Tang, Y. Reactive template-derived interfacial engineering of CoP/CoO heterostructured porous nanotubes towards superior electrocatalytic hydrogen evolution. *Carbon Energy* **2022**, *5* (1). DOI: 10.1002/cey2.273.

[21] Ghosh, P.; Kar, A.; Khandelwal, S.; Vyas, D.; Mir, A. Q.; Chakraborty, A. L.; Hegde, R. S.; Sharma, S.; Dutta, A.; Khatua, S. Plasmonic CoO-Decorated Au Nanorods for Photoelectrocatalytic Water Oxidation. *ACS Applied Nano Materials* **2019**, *2* (9), 5795-5803. DOI: 10.1021/acsanm.9b01258.

[22] Kim, J.-H.; Shin, K.; Kawashima, K.; Youn, D. H.; Lin, J.; Hong, T. E.; Liu, Y.; Wygant, B. R.; Wang, J.; Henkelman, G.; et al. Enhanced Activity Promoted by CeOx on a CoOx Electrocatalyst for the Oxygen Evolution Reaction. *ACS Catalysis* **2018**, *8* (5), 4257-4265. DOI: 10.1021/acscatal.8b00820.

[23] Li, W.; Zhao, L.; Wang, C.; Lu, X.; Chen, W. Interface Engineering of Heterogeneous CeO2–CoO Nanofibers with Rich Oxygen Vacancies for Enhanced Electrocatalytic Oxygen Evolution Performance. *ACS Applied Materials & Interfaces* **2021**, *13* (39), 46998-47009. DOI: 10.1021/acsami.1c11101.

[24] Luo, Y.; Yang, H.; Ma, P.; Luo, S.; Zhao, Z.; Ma, J. Fe3O4/CoO Interfacial Nanostructure Supported on Carbon Nanotubes as a Highly Efficient Electrocatalyst for Oxygen Evolution Reaction. *ACS Sustainable Chemistry & Engineering* **2020**, *8* (8), 3336-3346. DOI: 10.1021/acssuschemeng.9b07292.

[25] Sun, Z.; Liang, Y.; Wu, Y.; Yu, Y.; Zhang, B. Boosting Electrocatalytic Hydrogen-Evolving Activity of Co/CoO Heterostructured Nanosheets via Coupling Photogenerated Carriers with Photothermy. *ACS Sustainable Chemistry & Engineering* **2018**, *6* (9), 11206-11210. DOI: 10.1021/acssuschemeng.8b02676.

[26] Wang, D.; Du, Q.; Li, M.; Qian, L.; Wang, F. Ce-doped Co3O4 nanoplates for photo-assisted methanol electrocatalytic oxidation. *New Journal of Chemistry* **2024**, *48* (33), 14834-14843. DOI: 10.1039/d4nj02109f.

Acknowledgements

This research project was conducted over a six-month period at the Henan Institute of Advanced Technology, Zhengzhou University. It was made possible with the invaluable support of numerous individuals and organizations, and I would like to express my deepest gratitude to all those who contributed to its success.

First and foremost, I would like to thank my supervisor, Prof. Jingmin Ge, for her unwavering guidance, mentorship and encouragement throughout the entire research process. Prof. Ge played a crucial role in providing me with inspiration on the research topic, drawing from her extensive experience in electrocatalysis. Without her advice and keen insights, this project would not have been possible. Prof. Ge provided continual feedback on my self-developed experimental designs, and data analysis. She offered me very useful advice after I finished my first draft of my research article. Her guidance was provided on an unpaid, voluntary basis, highlighting her genuine commitment to student development and academic advancement.

In the initial phase of the project, I identified the research gap in the electrocatalytic oxidation of furfural, drawing from recent literature to pinpoint the potential application of Co_3O_4/NF. I carried out the actual experiments myself, including synthesizing the Co_3O_4/NF catalyst and conducting the electrochemical tests, while Prof. Ge provided critical feedback on the experimental procedures and troubleshooting when necessary.

Data collection for this project was a highly collaborative endeavor, involving a dynamic interplay between my hands-on experimentation and Prof. Ge's guidance. As the primary investigator, I took responsibility for acquiring the experimental results, meticulously conducting the synthesis of the Co_3O_4/NF catalyst and performing the subsequent electrochemical tests. This phase required a detailed and rigorous approach to ensure accuracy and reproducibility.

During the data analysis phase, we faced several significant challenges, particularly related to the accuracy of the electrochemical measurements. Unexpected fluctuations in the experimental setup posed issues that affected the reliability of our results. To address these challenges, I undertook a comprehensive review of the existing scientific literature to identify alternative data analysis techniques. This involved examining recent advancements in electrochemical measurement techniques and incorporating best practices from the literature. The insights gained led to

modifications in the experimental apparatus and analytical methods, which helped to minimize errors and enhance the precision of our data.

Regarding the report writing process, our roles were clearly defined. I independently drafted and optimized the initial versions of the report, focusing on presenting the experimental procedures, results, and interpretations in a clear and coherent manner. Prof. Ge's role was instrumental in providing critical revisions and suggestions, which involved detailed scrutiny of the draft to ensure the accuracy and clarity of the content. We engaged in several in-depth discussions to refine the report, addressing any issues to produce a comprehensive and polished final draft. This iterative process was crucial in meeting the highest academic standards and ensuring that the final report effectively communicated the significance and implications of our findings.

I would also like to extend my gratitude to Henan Institute of Advanced Technology, Zhengzhou University for their financial support and for providing access to the necessary research facilities. The advanced equipment provided by Henan Institute of Advanced Technology was essential for conducting the electrochemical experiments and characterizing the materials. Without their support, this research would not have been possible.

Lastly, I wish to thank the lab instructor Prof. Zhikun Peng as well as Mr. Jianyuan Deng for their guidance with the safety requirements during operation, as well as providing me with feedback and encouragement throughout the project. The collaborative spirit of this research not only made the process smoother but also enriched the overall experience.

This project was a rewarding learning experience, made possible through the combined efforts of all involved. I am deeply appreciative of everyone's contributions.